Robotica (2016) volume 34, pp. 1659–1676. © Cambridge University Press 2014
doi:10.1017/S0263574714002495

Water bouncing robots: a first step toward large-scale water running robots

Paolo Gallina*, Gabriele Bulian and Giovanni Mosetti

Department of Engineering and Architecture, University of Trieste, Trieste, Italy

(Accepted September 23, 2014. First published online: October 21, 2014)

SUMMARY

Robots running on water have attracted the attention of researchers in the last decades as an alternative to conventional aquatic propulsion mechanisms. Up to now, a large scale robot capable of running on water has not been realized. Bouncing on water is a prerequisite for running on water. For this reason, the development of a water bouncing robot represents a necessary first step. The paper presents the model of a 2-degree-of-freedom water bouncing robot inspired by the pogo-stick, a device for jumping off the ground in a standing position. An analytical model of the impact force between "robot's foot" and water is provided for both water-entry and water-exit phases. Such a model has been integrated in a dynamic simulation of whole robot. The model represents a useful and general framework to gain an insight into the parameters that characterize the efficiency of robot.

KEYWORDS: Aquatic propulsion; Water running; Aquatic robot; Water bouncing model; Slamming; Pogo-stick.

1. Introduction

Designing and building robots running on water is a challenging problem of interest for scientific community. So far the issue has been mainly faced on small and medium scales. A common approach consists in emulating some aspects of living systems, i.e. little animals capable of walking and running on water. Biomimetic robots are defined as biologically inspired robots. To this regard, Bush and Hu[1] classified water walkers according to their principal means of weight support and lateral propulsion. They analyzed the hydrodynamics of such creatures capable of sustaining themselves on water, exploiting surface tension effects. According to the biomimetic approach, Wang *et al.*[18] developed a bionic robot walking on water driven by a decoupled parallel mechanism. The robot was inspired by a water strider. A similar robot has been proposed by Zhang *et al.*[20] Shin *et al.*[16] also realized a robot inspired by a water strider. It is moved by means of shape memory alloy actuators and is capable of jumping out of water up to 26 mm. Both the aforementioned robots exploit the effect of surface tension at the interface between the water and the robot's footholds. This effect is present only on small scale robots since surface tension forces are negligible with respect to gravitational force and buoyancy on larger scale. Zhao *et al.*[21] developed a micro-robot that could continuously jump on water surface without sinking. The robot comprised three supporting legs and two actuating legs made from superhydrophobic nickel foam.

Pandey *et al.*[21] proposed a mechanical system for water locomotion inspired by frog's propulsion. They implemented a kinematic model that takes into account the kinematics of leg and foot. Floyd and Sitti[5] developed a robot that emulates the basilisk lizard's ability to run on the surface of water. The robot used a pair of identical four bar mechanisms, with a 180° phase shift to achieve locomotion on water's surface.[10] The robot has been designed taking into account the model of foot-to-water interaction related to lizard's shape and gate[7–9]: slap, stroke, and recovery phases. Slap phase occurs during the first impact with water. The impulsive generated force is based on the change in fluid's momentum. Stroke phase refers to the action of drugging the foot through water and pushing against

* Corresponding author. E-mail: pgallina@units.it

https://doi.org/10.1017/S0263574714002495 Published online by Cambridge University Press

it. It provides both lift and thrust. During the recovery phase the lizard removes the foot from the water. Shape of robot's feet has been optimized according to the lizard locomotion.[6]

All these robots are small scale robots. To the best of authors' knowledge, there have been no attempts to develop large scale water running robots. There exist several reasons for this: Dynamic balancing during running tasks is much more challenging in water than on ground; experimental apparatus are more difficult and critical to realize because of water; and, most of all, the parameters involved in the mechanism of running on water are not completely understood, especially during the jumping phase. Nature itself teaches that scale effects are dominant on the evolution of creatures capable to run on water. For example, Glasheen and McMahon[7–9] found an interesting relationship between scale of basilisk lizards and their ability to run on water. In particular, small lizards can generate an upward impulse, which doubles when needed to support their body. Conversely, larger lizards (up to 0.1 kg) can just barely support their bodies and are not good runners.

This paper aims to partially fulfill this gap by providing useful and simple guidelines to the design of large scale water running robots. Although it focuses on the simplified case of a 2-degree-of-freedom (DoF) jumping robot, its results, as well as the proposed efficiency indices, are valid for more general robots. Several definitions could be given for "water running robots." In the following, a water running robot is defined as a mechanism capable of moving on water (running) by a sequence of jumps (out of water, i.e. during the jump phase, for a short time, no component of mechanism has to be in contact with water), exploiting the upward impulsive force due to the impact of robot's foot on water. According to this definition, a strider-like robot floating on water and capable to perform single jump (or single stride) once in a while is not considered a water running robot.

The proposed large scale model is inspired by the pogo-stick toy used to jump efficiently on ground. High jumping efficiency is due to the presence of spring that can accumulate energy exploited afterwards during the upward phase. This characteristic has been integrated in the proposed robot. At the same time, it has been adapted to take into account the fluid-structure interaction.

The paper is organized as follows. In Section 2, a general presentation of the pogo-stick-inspired concept is presented. Section 3 describes the dynamic model of mechanism. The modeling of fluid-structure interaction force is described in Section 4, and validated through some experimental results in Section 5. Eventually, Section 6 shows simulation results of the dynamic model integrated with the fluid-structure model and discusses the proposed indices.

2. Pogo-Stick-Inspired Robot

Since running on water is a complex and critical task (few living creatures have this skill), it is necessary to select a proper base mechanism to achieve high efficiency. The one we propose is a 2-DoF water bouncing mechanism that uses an elastic element as an energy storage device. Unlike the majority of water running robots presented in literature, it is not inspired biologically by a living creature but by a combination of person and the pogo-stick toy. Pogo-stick is a toy for jumping off the ground in a standing position (see Fig. 1 left). It is used because, thanks to the spring interposed between pogo-stick's base (called "foot" in the following) and the person's feet, the person is capable to perform higher jumps than barefooted. A simplified dynamic model of pogo-stick plus the person is sketched in Fig. 1 (center). It consists of a 2-DoF lumped element model. Three masses are considered: mass of a pogo-stick, mass of the legs and part of the trunk (down-mass), and mass of shoulders, head, and chest (up-mass). The jump occurs when the person repetitively moves the up-mass with respect to the down-mass at a given frequency and with a given amplitude. Such an action is amplified by the presence of a spring. Coming to the case of water, such a model could be modified considering that pogo-stick's foot has to be replaced with another "foot," which is capable to interact with water in the sense that it has to provide high upward forces during downward motion (impact with water) and low resistance forces during exit-from-the-water motion. For example, in Fig. 1 on the right, the foot of a water jumping robot consists of a cone.

It is evident that other typologies of feet, such as flat feet, geometrically varying shape of feet, ball feet, upside-down cup feet, etc., could be employed. Nevertheless, we believe that cone is still a good candidate to gain an insight into the jumping phenomenon for several reasons. First, thanks to its radial symmetry, the shape is very suitable for this investigation, where only the vertical motion of the system is considered. Second, this shape has been broadly investigated when addressing water-impact problems. Third, the shape depends on a single parameter (i.e. the deadrise angle). More complicate

https://doi.org/10.1017/S0263574714002495 Published online by Cambridge University Press

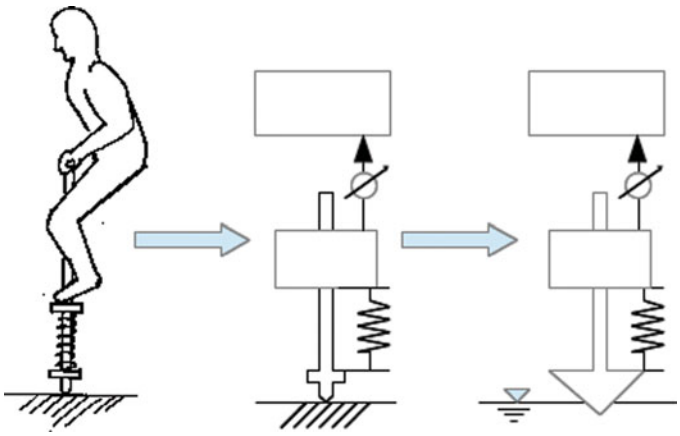


Fig. 1. The 2-DoF water bouncing robot.

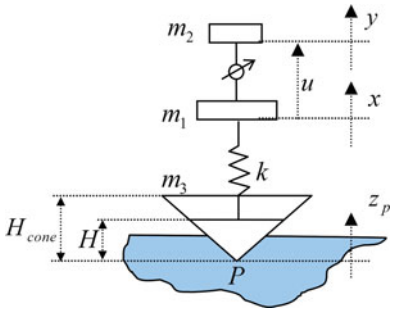


Fig. 2. Dynamic 2-DoF model of the water bouncing robot.

foot shapes could be more efficient (such as geometry varying shape of feet) but at the same time would require the analysis of other parameters, thereby increasing the complexity of the model. In this work, instead of the definitions of slap, stroke, and recovery phases used to describe the single stride of lizard-inspired robots, the notion of water-entry and water-exit phases is employed. Water-entry phase begins when the robot's foot enters the water during downward motion. Water-exit phase follows, and it begins when the motion reverses direction (upward motion). It ends when the robot's foot detaches from the water.

The mechanism can simulate just the jump out of water on the vertical direction. But the concept could be easily extended to the case of more degrees of freedom mechanisms and/or mechanisms with more locomotion legs (biped or four-leg locomotion mechanisms). In any case, before designing and developing two-leg or four-leg water running robots exploiting the pogo-stick concept, it is necessary to assess the concept itself and the contribution to an efficient jump, which is given by different physical parameters. For this reason a simplified analytical model of the impact force between robot's foot and water is provided, as well as its integration with the dynamic model of the masses connected to the foot by means of elastic element.

3. Two-DoF Dynamic Model of Robot

The dynamic model of 2-DoF water bouncing robot is given in Fig. 2. Only the vertical motion is considered; x, y, and z_p are respectively the vertical position of the main mass of robot (m_1), the vertical position of the active mass (m_2), and the vertical position of robot's foothold (m_3).

A spring of stiffness k connects the two free masses. According to the metaphor of the pogo-stick game, mass m_3 (the cone) represents the mass of pogo-stick's foot, m_1 is the mass of person's body (legs and pelvis), and m_2 is the mass of person's trunk. The jumping action is generated by the motion of the trunk with respect to the inferior part of legs, and it is amplified by the action of spring.

https://doi.org/10.1017/S0263574714002495 Published online by Cambridge University Press

At the same time, for the proposed robot, an actuator is embedded between the mass m_1 and m_2. The scope of the actuator is to provide appropriate forcing to create jumping action (i.e. the jumping off the water by the cone) by imposing the relative motion of the mass m_2 with respect to the mass m_1. Such a dynamic action is amplified by the interposed spring. Therefore, it is assumed that the relative distance

$$u = y - x \tag{1}$$

can be controlled during time. By applying the vertical dynamic equilibrium to all the rigid bodies of robot, it is easy to carry out the following dynamic system:

$$\begin{bmatrix} m_1 + m_2 & 0 \\ 0 & m_3 \end{bmatrix} \begin{Bmatrix} \ddot{x} \\ \ddot{z}_p \end{Bmatrix} + \begin{bmatrix} k & -k \\ -k & k \end{bmatrix} \begin{Bmatrix} x \\ z_p \end{Bmatrix} = \begin{Bmatrix} -(m_1 + m_2)g - m_2\ddot{u} + k\ H \\ -m_3 g + F_z - k\ H \end{Bmatrix}, \tag{2}$$

where g is the gravitational acceleration, H is the height of the spring connection point above the vertex P of the cone, F_z is the nonlinear interaction force between the cone and the water, which is discussed in more detail in the following sections of the paper.

The shape of the body interacting with the water is conical. This choice presents several advantages. First of all, it allows developing an approximate analytical model of the fluid-structure interaction force. In addition, it represents a trade-off between water-entry force and water-exit force. In fact, a high water-entry force is preferred since it prevents the robot from sinking during the impact. Moreover, a low water-exit force is preferred since it does not counteract the jumping off the water phase. If a disk is employed in place of a cone, water-entry force and water-exit force would be higher. Conversely, if a foothold ending in a very sharp point is employed, water-entry force and water-exit force would be lower.

4. Fluid-Structure Interaction Force, F_z

In order to simulate the behavior of robot, it is necessary to implement a modeling for the fluid-structure interaction force. Since the aim of the study is to have a robot able to bounce on water, the modeling must be able to provide forces for both water-entry and water-exit phases. The water-entry phase is that phase of motion when the (conical) base of the robot moves downwards, passing from a condition with the (conical) base completely in air to a condition with the (conical) base partially in water. Conversely, the water-exit phase is the phase when the (conical) base of the robot, being partially in water, moves upwards.

In general, the water-entry/water-exit problem is a complex fluid-structure interaction problem, characterized by free surface fragmentation, jets, high localized impact pressures, possibility of air entrapment, etc.[3] In case highly accurate results are needed, such phenomena should be modeled by means of computational fluid dynamics tools, or direct experiments should be performed.

Such approaches, however, were considered unsuitable for the present study. This study is indeed preliminary in nature, and it is aimed at exploring the dynamics of the system through extensive simulations with the goal of finding a set of system parameters that could likely lead to the actual "bouncing" of robot. CFD computations and experiments are too time-consuming for this purpose, and cannot be used in an extensive initial exploration phase of dynamical system.

In order to overcome this difficulty, it was then decided to implement a simplified modeling technique, which is described later, with the intention of balancing simplicity/computational speed and accuracy. The fluid-structure interaction force was thus modeled making use of approximate methods based on potential flow assumption. Such approaches are often used in the field of naval architecture to provide impact forces during the so-called slamming events, i.e. violent entrance in water, with consequent impulsive pressures (impacts), of some parts of ship (typically the bow or the stern). This phenomenon typically occurs when relative ship-wave motions are significant.

Hence, for the present study, the force arising in the water-entry and water-exit phases was modeled using the background from refs [3, 17, 19]. The idea of the present modeling is to treat the water impact problem, i.e. the water-entry phase, by using the classical von-Karman approach[17] but adding a draught-independent swell-up correction in the instantaneous draught of body, which makes the

https://doi.org/10.1017/S0263574714002495 Published online by Cambridge University Press

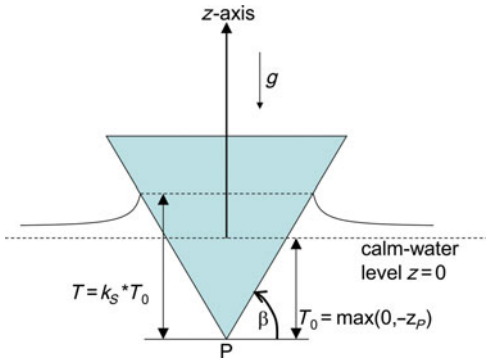


Fig. 3. Main geometrical parameters for the modeling of the fluid-structure interaction force.

approach a Wagner-type method.[19] The water-exit phase is modeled according to Faltinsen[3] and Piro and Maki[14] by neglecting the so-called "impact term."

In the analysis of high speed water-impact problems of blunt bodies, the buoyancy, i.e. the force arising due to hydrostatic pressure, is often neglected, since it is small compared with the impact force.[3] However, in this study such approximation cannot be made, and modeling of buoyancy is necessary. This is due to the fact that the body used (the foot of the robot) cannot strictly be considered a blunt body, and because the exploration of the system is carried out in a wide range of parameters, and for some combinations of parameters the robot remains in water without performing subsequent water-entrance/water-exit phases (i.e. without bouncing). In such conditions the buoyancy force is fundamental and must be taken into account in order to have a consistent, though approximate, fluid-structure interaction force model.

In the developed modeling, wave radiation is not considered. This is in line with the underlying assumptions of impact model, which basically assumes a constant potential on free surface.[3] However, in a real case, some waves will be generated. In an unbounded domain, such waves will then propagate from the impact point toward infinity. Herein, it is assumed that the lack of modeling of free surface disturbance, and consequent fluid-free surface-structure interaction, is an acceptable simplification in view of the scope of the study. In order to overcome this limitation in modeling, particularly in the case of multiple jumps, it seems necessary to make use of much more complex direct computational fluid dynamics approaches, which, as reported before, are too time-consuming and therefore unsuitable for the purpose of the present study. When applying the considered modeling, and when looking at the obtained results, it is therefore necessary to bear in mind the mentioned limitation.

4.1. Geometry and general fluid-structure interaction force model

A sketch of the geometry of the problem showing the main parameters of modeling of fluid-structure interaction force is reported in Fig. 2. The body is considered to be free to move in 1 DoF, i.e. the vertical direction.

With reference to Fig. 3, in general, a laterally symmetric 2D or an axisymmetric 3D object impacting the water is considered. Herein, for convenience, the calm water level is set to $z = 0$. In the classical von-Karman approach,[3,17] calculations are based on the calm water level. However, as shown by Wagner[19] and Faltinsen,[3] and as also everyone's experience shows, the entrance of a body in water generates a swell-up. Under certain approximations, the swell-up effect can be quantified starting from the body geometry.[4] Lateral jets are also generated, which are not explicitly considered in this model (see refs. [2–4]). As a result of the swell-up effect, the contact point between the body and the water surface (neglecting jets) is at a level higher than the calm water level.

In general, at the cost of a complication of modeling, the local contact point between the free surface and the body surface could be determined by means of Wagner's approximate theory.[4,19] Herein, it is considered sufficient to reproduce the swell-up phenomenon by means of a proportional increase in the nominal (i.e. without swell-up effect) local draught of the object.

https://doi.org/10.1017/S0263574714002495 Published online by Cambridge University Press

The nominal draught T_0 of the object with respect to the calm water level $z = 0$ can be written on the basis of the vertical coordinate z_P of the lowest point P as:

$$T_0 = \max(0, -z_P). \tag{3}$$

In order to take into account the swell-up effect, a swell-up coefficient k_S is introduced, which links the actual draught T up to the water-body contact point and the nominal draught:

$$T = k_S \cdot T_0 = k_S \cdot \max(0, -z_P). \tag{4}$$

The modeling for the fluid-structure interaction force is considered separately for two different phases[3,14]:

- The entrance/downwards phase, where it is assumed that an impact occurs.
- The exit/upwards phase, where the impact term is neglected.

The instantaneous force F_z acting on the body during the water entrance phase is written as[3]

$$\begin{aligned} F_z &= -\frac{d}{dt}(A_{33}(T) \cdot V) + F_{\text{buoyancy}}, \\ V &= \dot{z}_P < 0. \end{aligned} \tag{5}$$

The first term represents the force associated with the variation of the fluid momentum due to the action of the body entering the water. Such first term embeds the so-called "slamming" force and the force associated with the "usual" linear added mass force. The second term represents the contribution from the buoyancy, and this will be discussed later in some more detail. $A_{33}(T)$ is the high-frequency (infinite frequency) hydrodynamic-added mass. In order to take into account the swell-up effect, the added mass is assumed to be evaluated at a draught equal to the instantaneous (corrected) draught T (see Eq. (4)). Since a vertically translating rigid body is considered, the instantaneous entrance (impact) speed V coincides with the speed $\dot{z}_P$ of the lowest point P. Such speed is negative, i.e. $\dot{z}_P < 0$, during the water-entry phase of the motion. By recognizing that

$$\begin{cases} \frac{d}{dt}(A_{33}(T) \cdot V) = \frac{d}{dt}(A_{33}(T)) \cdot \dot{z}_P + A_{33}(T) \cdot \ddot{z}_P, \\ \frac{d}{dt}(A_{33}(T)) = \frac{d}{dT}(A_{33}(T)) \cdot \frac{dT}{dt} = \frac{d}{dT}(A_{33}(T)) \cdot k_S \cdot \frac{dT_0}{dz_P} = -\frac{d}{dT}(A_{33}(T)) \cdot k_S \cdot \dot{z}_P, \end{cases} \tag{6}$$

the force during the ingress phase in Eq. (5) can be further rewritten as

$$\begin{aligned} &F_z = -\frac{d}{dt}(A_{33}(T) \cdot V) + F_{\text{buoyancy}} = -\frac{d}{dT}(A_{33}(T)) \cdot k_S \cdot \dot{z}_P|\dot{z}_P| - A_{33}(T) \cdot \ddot{z}_P + F_{\text{buoyancy}} \\ &\text{when } \dot{z}_P < 0. \end{aligned} \tag{7}$$

As also described by Faltinsen,[3] the force during the ingress phase in Eq. (7) is therefore given by the following three contributions:

1. The impact (slamming) force, which is the term $-\frac{d}{dT}(A_{33}(T)) \cdot k_S \cdot \dot{z}_P|\dot{z}_P|$ and depends on the shape of the body (through the term $\frac{d}{dT}(A_{33}(T))$), the square of the instantaneous velocity $\dot{z}_P$, and on the swell-up effects (through the swell-up correction coefficient k_S).
2. The "standard" added mass force, which is the term $-A_{33}(T) \cdot \ddot{z}_P$.
3. The buoyancy force F_{buoyancy}, which depends on the shape of the body.

During the exit phase, i.e. when $\dot{z}_P > 0$, it is usual to model the force by neglecting the impact (slamming) term.[3,14] Therefore, the force in the exit phase takes the following form:

$$\begin{aligned} &F_z = -A_{33}(T) \cdot \ddot{z}_P + F_{\text{buoyancy}} \\ &\text{when } \dot{z}_P \geq 0. \end{aligned} \tag{8}$$

https://doi.org/10.1017/S0263574714002495 Published online by Cambridge University Press

It is worth mentioning at this stage some similarities and differences between the general model used herein (Eqs. (6)–(8)) and the modeling developed in the past by Glasheen and McMahon[7–9] to analyze the water-running capability of the basilisk lizard. First of all it is necessary to underline that the modeling by Glasheen and McMahon[7–9] is based on the impact of a flat plate (representing the foot of the basilisk lizard), which, during the water entrance, generates an air cavity behind itself. Such modeling is justified by the observation that this is the actual physical phenomenon occurring in reality when the basilisk lizard runs on water. In the modeling herein, instead, it is assumed that the geometrical shape of the foot is not to generate any air cavity or air entrapment, and a fully single phase potential model is employed. Also, the modeling by Glasheen and McMahon[7–9] is mainly intended as an analysis model, while the model herein is intended, mostly, as a simplified initial design/explorative model. As a result, the model by Glasheen and McMahon[7–9] is accurate and specific for the analyzed case, while the model herein is of more general applicability.

In particular, the model is intended for being possibly used to different shapes of robot feet. Another difference between the two modeling approaches is the fact that, while Glasheen and McMahon[7–9] mostly concentrate on an impulsive approach, i.e. an analysis based on change of momentum and consequent force impulse, the model developed herein is intended for an application in time domain simulations. Despite these main differences, there are however some direct and indirect similarities. The first similarity between the two modeling approaches is associated with the fact that in both the approaches part of the fluid-structure interaction force is due to change in fluid momentum, while another part of the fluid-structure interaction force is due to hydrostatic pressure. In the present case the two effects are explicitly separated, and the hydrostatic pressure is naturally embedded in the model, since a large scale rigid foot is assumed, which is subject to dynamic and hydrostatic pressure. In case of the modeling of Glasheen and McMahon,[7–9] the two effects are embedded in the same drag coefficient, and the effect of the hydrostatic pressure acting on the bottom of the impacting plate enters into play as a consequence of the presence of the air cavity generated behind the plate during the entrance phase. As a result, part of the fluid-structure interaction force in the modeling by Glasheen and McMahon[7–9] is generated by the unbalancing of the hydrostatic pressure between the lower part (which is in contact with water) and the upper part of the plate (which is in contact with the air in the open cavity). The two modeling approaches also share a similarity regarding the effect of surface tension, which herein is totally neglected, while it is proved to have negligible effects at the object scales and dynamic conditions considered by Glasheen and McMahon.[7–9]

4.2. Model details and parameters in case of a cone

The simplified fluid-structure interaction force model described in Eqs. (5)–(8) is general in nature. However, its parameters need to be specified for a particular geometry of the base of the robot which was used in this study, i.e. a cone.

From the hydrodynamic point of view, it is necessary to know the high frequency added mass, $A_{33}(T)$, and the swell-up coefficient, k_S.

Following Faltinsen and Zhao,[4] the swell-up coefficient k_S was taken equal to the approximate theoretical value for cones with small deadrise angles β (as defined in Fig. 3):

$$k_S = \frac{4}{\pi}. \tag{9}$$

Regarding the high frequency added mass, $A_{33}(T)$, first it is to be noted that the cone is a self-similar geometric shape. As a consequence, it follows that, for any generic draught T, the high frequency added mass can always be written by means of a dimensionless added mass coefficient as follows:

$$\begin{aligned} A_{33}(T) &= k_{a33}(\beta) \cdot \rho \cdot \Omega(T), \\ \Omega(T) &= \frac{\pi \cdot R(T)^2 \cdot T}{3} = \frac{\pi \cdot T^3}{3 \cdot \tan^2(\beta)} = \frac{\pi \cdot R(T)^3 \cdot \tan(\beta)}{3}. \end{aligned} \tag{10}$$

In Eq. (10), ρ is the fluid density (kg/m^3), the cone base radius at a draught T is indicated as $R(T)$, $\Omega(T)$ is the cone volume at the generic draught T, and $k_{a33}(\beta)$ is the dimensionless added

https://doi.org/10.1017/S0263574714002495 Published online by Cambridge University Press

Table I. Numerically calculated added mass coefficient for different deadrise angles.

Deadrise angle, β	0°	10°	20°	30°	40°	50°	60°
$\frac{A_{33}}{\frac{4}{3}\cdot\rho\cdot R^3}$	1.00 (analytical)	0.96	0.89	0.81	0.74	0.67	0.59

mass coefficient. This latter, thanks to the mentioned self-similarity of the cone, depends only on the deadrise angle β.

In the limit of small deadrise angles, the high frequency added mass coefficient $k_{a33}(\beta \to 0)$ could be approximated as that of a disk at water surface. This latter, in turn, can be determined from half the added mass coefficient of a fully submerged disk. Hence, following refs. [3, 11, 12, 15],

$$\beta \to 0 \Rightarrow A_{33} \approx \frac{4}{3} \cdot \rho \cdot R^3(T) \Rightarrow k_{a33} \approx \frac{4}{\pi \cdot \tan(\beta)}. \tag{11}$$

In this study, instead of using the small deadrise angle approximation in Eq. (11), it was decided to numerically determine the added mass coefficient as half of that of a fully submerged double cone using the three-dimensional potential boundary element method. Since the deadrise angle was one of the parameters to be used in the initial exploration of dynamical system, different deadrise angles were considered in the calculations, from 10° to 60°. The theoretical result in Eq. (11), i.e. for $\beta \to 0^\circ$, was also added to supplement direct numerical calculations. Results from such calculations are shown in Table I.

Considering Eq. (10), it can be noted that for a self-similar shape as a cone (similarly for a two-dimensional wedge), it is

$$\begin{aligned} \frac{d}{dT}\left(A_{33}(T)\right) &= k_{a33}(\beta) \cdot \rho \cdot \frac{d}{dT}\Omega(T) = k_{a33}(\beta) \cdot \rho \cdot A_w(T), \\ A_w(T) &= \pi \cdot R(T)^2 \text{ for a cone,} \end{aligned} \tag{12}$$

where $A_w(T)$ is the water plane area at draught T.

When it comes to the modeling of the buoyancy term F_{buoyancy} (see Eqs. (5), (7), and (8)), at the first glance it would seem appropriate to model it as the force due to the hydrostatic pressure up to the draught T, i.e. the draught corrected for swell-up effects. Although such a model can be considered as an appropriate approximation for a motion characterized by an actual continuous bouncing in and out of water, or at least in case of the entrance phase, the same model would not provide the correct hydrostatic equilibrium in absence of motion, i.e. with the object at rest. As a result, it was considered more robust, in this phase of the study, to approximate the buoyancy force without taking into account the swell-up. The model for the buoyancy force was then considered to be:

$$F_{\text{buoyancy}} = \rho \cdot g \cdot \Omega(T_0). \tag{13}$$

4.3. Final model in case of the considered cone

By taking into account all the considerations made up to this point, the final fluid-structure interaction force model takes the following form:

$$\begin{aligned} &F_z = -\rho \cdot A_w(T) \cdot k_{a33}(\beta) \cdot k_S \cdot k_{\text{phase}} \cdot \dot{z}_P|\dot{z}_P| - k_{a33} \cdot \rho \cdot \Omega(T) \cdot \ddot{z}_P + \rho \cdot g \cdot \Omega(T_0) \\ &\text{with} \\ &k_{\text{phase}} = \begin{cases} 1 & \text{if } \dot{z}_P < 0 \text{ (ingress phase)} \\ 0 & \text{if } \dot{z}_P \geq 0 \text{ (exit phase)} \end{cases}, \\ &k_S = \frac{4}{\pi};\ k_{a33}(\beta) : \text{from direct calculation,} \end{aligned} \tag{14}$$

https://doi.org/10.1017/S0263574714002495 Published online by Cambridge University Press

$$A_w(T) = \pi \cdot \left(\frac{T}{\tan\beta}\right)^2 = \pi \cdot k_S^2 \cdot \left(\frac{T_0}{\tan\beta}\right)^2 = \pi \cdot k_S^2 \cdot \frac{[\max(0, -z_P)]^2}{\tan^2\beta},$$

$$\Omega(T_0) = \frac{1}{3} \cdot A_w(T_0) \cdot T_0 = \frac{\pi}{3} \cdot \frac{[\max(0, -z_P)]^3}{\tan^2\beta}.$$

Although model (14) can be used in case of small deadrise angles (i.e. for small values of β), it is not possible to use it in the singular case of a disk ($\beta = 0$). However, in case of small but non-zero values of the deadrise angle, $k_{a33}(\beta)$ can be approximated by using Eq. (11).

It is important to note that the developed model is intended to approximately represent the fluid-structure interaction during impact events, and in particular from the moment of impact, for the following downward motion phase and then for the subsequent upward motion phase. In such conditions, wave radiation effects are negligible, and therefore have not been modeled in Eq. (14) to keep the model as simple as possible. With the aim at arriving at steady impact conditions, the fluid-structure interaction model can still be used for temporarily simulating transient conditions when the object oscillates around a hydrostatic equilibrium position, or, in general, transient conditions when the object is permanently immersed. When so used, however, it must be borne in mind that the fluid-structure interaction model is not dissipative or, at best, not as dissipative as reality, since the fluid-structure interaction model does not embed energy dissipation, which, in such conditions, is due to wave radiation.

5. Validation of Fluid-Structure Interaction Force Model

The fluid-structure interaction force model has been validated through free fall experimental results. Two cones with different deadrise angles ($\beta = 31^\circ$ and 45°) have been considered. The center of the base of each cone was fastened to a cylindrical hollow brass rod (295-mm long and 8 mm in diameter). The rod was vertically guided by means of two low friction rings, made of Teflon and spaced out of 110 mm. An 8-mm edge iron cube was connected to the head of the rod and a piezoelectric accelerometer (PCB 352-C22) was connected to the cube by means of petro-wax. The cone-rod piece was held to a constant distance from water by means of a clamp and quick-release mechanism.

For each test, the cone was released from an initial height above the water surface (0.113 m for the case $\beta = 31^\circ$ and 0.093 m for $\beta = 45^\circ$). The free falling mass was different for the two cones: 0.14 kg for $\beta = 31^\circ$ and 0.18 kg for $\beta = 45^\circ$. After it was released (free fall motion) the acceleration was recorded. For the smaller deadrise angle, the plot of deceleration (caused by the fluid-structure interaction force F_z) versus time is reported in Fig. 4 (top plot). The test has been repeated for five times for each case. Each colored line represents a different test repetition. Raw acceleration signals have been then low-passed and the resulting filtered acceleration signals are given in the bottom plot of Fig. 4.

The black solid line in Fig. 4 represents the acceleration obtained by the implementation of the dynamic model (2). Since a free fall motion is considered, the actuator force was null ($\ddot{u} = 0$).

Note that simulation results match experimental ones, at least during the beginning of the water-entry phase. Some discrepancies are visible at the end of the time history, where, however, for the considered cone, water overtopping was occurring, which is a phenomenon not taken into account by the simplified approximate fluid-structure interaction force model, and which can in any case be avoided by increasing the total height of the cone H_{cone}.

Figure 5 shows a similar comparison of experimental and simulated results for the cone with deadrise angle, $\beta = 45^\circ$. Also in this case, experimental and simulated results match during the water-entry phase. Note that the deceleration values in Fig. 5 are lower than the ones in Fig. 4 as expected. Indeed, the higher the deadrise angle, the lower the fluid-structure impact force and the deceleration undergone by the cone.

The Weber number for the two cases has been calculated to check the relative importance between inertial effects and surface tension effects (see also ref. [7]. In the calculation, the reference speed has been considered to be the nominal speed at the moment of impact with water, the reference length has been considered to be the cone radius at water plane at hydrostatic equilibrium, and the surface tension has been taken as equal to 0.072N/m (fresh water at 25° C). The resulting Weber number is 1.4×10^3

https://doi.org/10.1017/S0263574714002495 Published online by Cambridge University Press

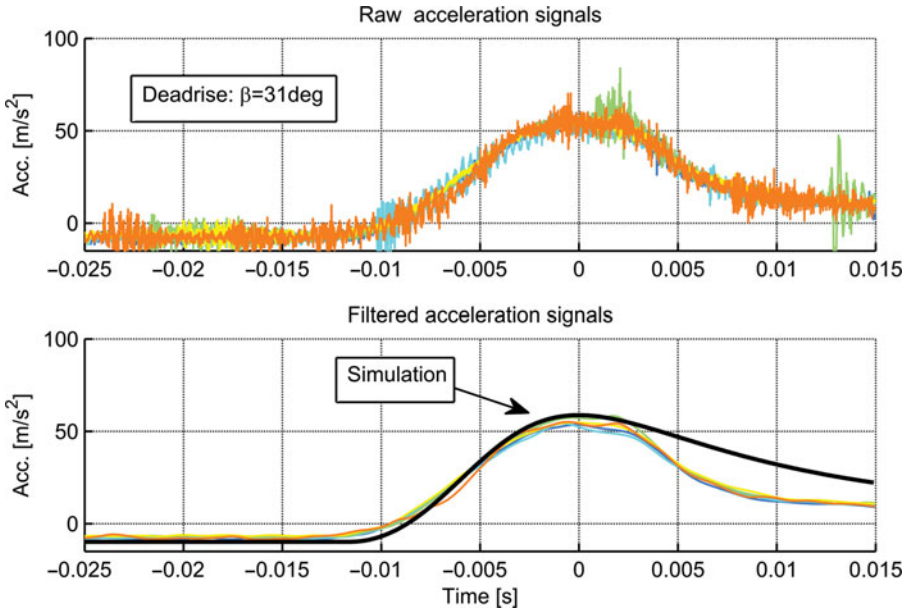


Fig. 4. Deceleration during water-entry phase for a cone with a deadrise angle of 31°. Experimental results versus simulation results. Each test repetition is represented by a different line color.

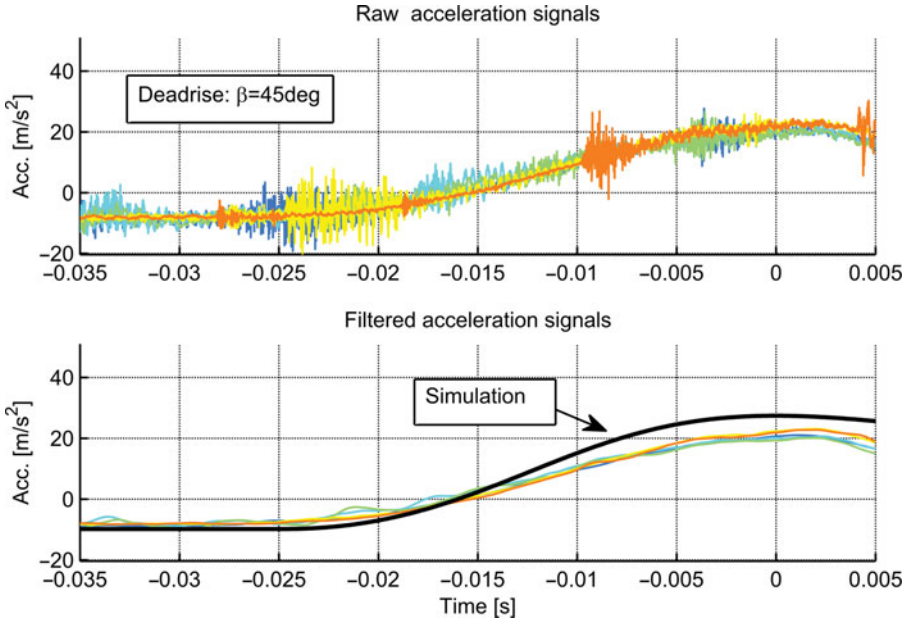


Fig. 5. Deceleration during water-entry phase for a cone with a deadrise angle of 45°. Experimental results versus simulation results. Each test repetition is represented by a different line color.

for $\beta = 45°$, and 1.9×10^3 for $\beta = 31°$. Such high values indicate the negligible contribution of surface tension effects. For the sake of reference, the Froude number calculated by using the same reference speed and reference length turns out to be 1.8 for $\beta = 45°$ and 1.9 for $\beta = 31°$, while the Reynolds number calculated using the same reference speed and length, and considering a kinematic viscosity of $0.9 \cdot 10^{-6}$ m^2/s is 0.8×10^5 for $\beta = 45°$, and 1.0×10^5 for $\beta = 31°$.

6. Simulation Results

As can be easily guessed, the possibility of jumping out of water depends upon many dynamic and geometrical parameters: feet shape, value of mass, stiffness of spring, and input forces. Not

https://doi.org/10.1017/S0263574714002495 Published online by Cambridge University Press

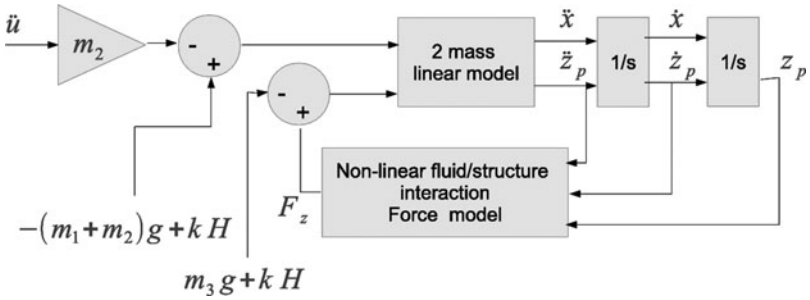


Fig. 6. Simulation conceptual schema.

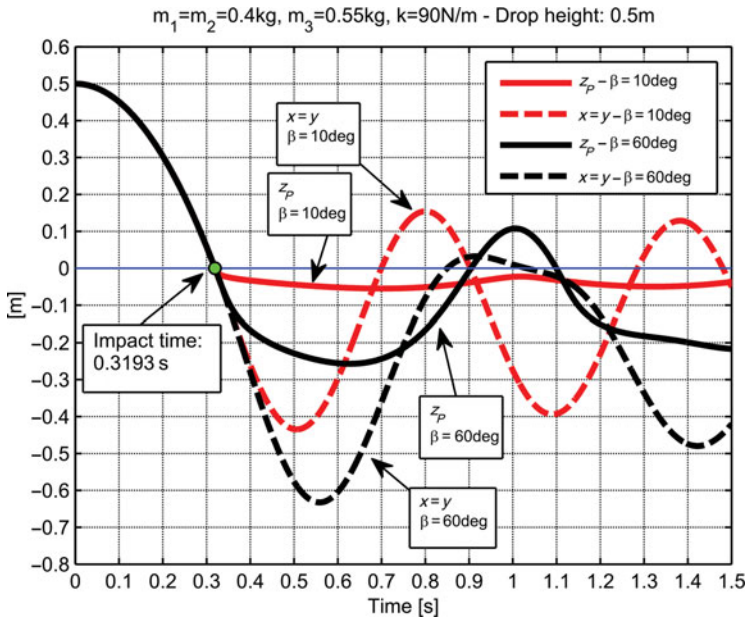


Fig. 7. Example simulations of passive ($\ddot{u} = 0$) drop test for two deadrise angles: $\beta = 10^\circ$ and 60°. The other parameters are constant: $m_1 = m_2 = 0.4$ kg, $m_3 = 0.55$ kg, $k = 90$ N/m. Jumping off water occurs only for the case $\beta = 60^\circ$. For $\beta = 10^\circ$, hydrodynamic forces prevent the exit of robot's foot from water.

all the parameter combinations are acceptable. In many cases, a wrong choice of parameter values prevents the robot from jumping out of water. The goal of the implemented simulation consists in exploring the role of some of the parameters, trying to identify the dominant ones as well as the regions of the parameters that are more likely to allow an efficient jumping action. Figure 6 shows the general schema of simulation. The external forcing that represents the input to the system is given by the acceleration $\ddot{u}$ imposed by the actuator. The two-mass linear dynamic model interacts with the nonlinear fluid-structure model through acceleration, speed, and position data values. With reference to Fig. 2, it will be assumed in the following that $H = 0$ (i.e. the spring is nominally connected to the vertex of the cone) and that H_{cone} is always sufficiently large to avoid full submergence of robot's foot. In all simulations, fresh water is assumed with a mass density, $\rho = 1000$ kg/m^3.

6.1. Passive free fall, single jump test

Let us first consider just a passive free fall, single jump test: The simulation consists in releasing the robot from a certain height of the water level ($x(t = 0) = y(t = 0) = z_P(t = 0) > 0$) with zero initial velocity ($\dot{x}(t = 0) = \dot{y}(t = 0) = \dot{z}_P(t = 0) = 0$). Moreover, no external energy is provided to the robot ($\forall t \geq 0, u(t) = 0$). Two example simulations have been carried out for two different deadrise angles: 10° and 60°. Mass values and spring constant as well as the initial dropping height have been kept the same for both the cases. Simulation data and results of simulations for these two cases are shown in Fig. 7.

https://doi.org/10.1017/S0263574714002495 Published online by Cambridge University Press

Once the robot impacts the water, the upward impact force tends to decelerate the cone. The fluid-structure interaction force, which also comprises the hydrostatic buoyancy force, eventually inverts the downfall motion. During downfall cone motion, energy is stored in the spring mass sub-system as well, thanks to the buoyancy (which is a conservative force), and this energy is then released in the upward motion phase. In case the downward added mass force dominates the exit phase, the cone is not able to jump out of water, and this happens, in the example given in Fig. 7, for $\beta = 10^\circ$. Instead, when the combined effect of buoyancy and the spring-mass sub-system is sufficient to overcome added mass forces in the exit phase, the system can jump out of water, and this happens, in the example given in Fig. 7, for $\beta = 60^\circ$.

This kind of simulation is useful to characterize the capacity of robot to jump out of water in a passive way, i.e. without any external energy provided. Our assumption is that if the robot exhibits high efficiency on a single passive jump, it can also run with high efficiency if a proper actuation effect $u(t)$ is introduced. The efficiency of passive jump can be quantified from simulations by analyzing the energy dissipated in a jump when the robot is able to passively jump out of water. Slamming force, added mass force, and the capacity to store energy (and release it at right moment) are the three major aspects involved in the jump. The first two are related to foot's shape; for the cone case, slamming force and added mass force depend on the deadrise angle. The third is basically related to the stiffness coefficient. It shall also be recalled that the buoyancy force, being a conservative force, also stores and releases energy during the jump, and that the buoyancy force depends on the deadrise angle of robot's foot. Therefore, analyzing mutual effects of the deadrise angle β and the spring stiffness k is strategic.

The energy of the robot at the beginning of the water-entry phase, i.e. for $t = t_{\text{in}}$ when the impact occurs, is (note that the robot's foot at the moment of impact is out of water) as follows:

$$
\begin{aligned}
&E_{\text{out}} = E\left(t = t_{\text{in}}\right) = K_1\left(t_{\text{in}}\right) + K_2\left(t_{\text{in}}\right) + K_3\left(t_{\text{in}}\right) + U_{g,1}\left(t_{\text{in}}\right) + U_{g,2}\left(t_{\text{in}}\right) + U_{g,3}\left(t_{\text{in}}\right) + U_k(t_{\text{in}}),\\
&K_1 = \frac{m_1 \cdot \dot{x}_{\text{in}}^2}{2}; \quad U_{g,1} = m_1 \cdot g \cdot x_{\text{in}}; \quad K_2 = \frac{m_1 \cdot \dot{y}_{\text{in}}^2}{2}; \quad U_{g,2} = m_2 \cdot g \cdot y_{\text{in}};\\
&K_2 = \frac{m_1 \cdot \dot{z}_{P,\text{in}}^2}{2}; \quad U_{g,3} = m_2 \cdot g \cdot z_{P,\text{in}} \overbrace{=}^{z_P(t_{\text{in}})=0} 0; \quad U_k = \frac{1}{2} \cdot k \cdot \left(x_{\text{in}} - z_{P,\text{in}}\right)^2 \overbrace{=}^{z_P(t_{\text{in}})=0} \frac{1}{2} \cdot k \cdot x_{\text{in}}^2
\end{aligned}
\tag{15}
$$

with

$$
\begin{aligned}
x_{\text{in}} &= x(t_{\text{in}}); \quad \dot{x}_{\text{in}} = \dot{x}(t_{\text{in}});\\
y_{\text{in}} &= y(t_{\text{in}}); \quad \dot{y}_{\text{in}} = \dot{y}(t_{\text{in}});\\
z_{P,\text{in}} &= z_P(t_{\text{in}}); \quad \dot{z}_{P,\text{in}} = \dot{z}_P(t_{\text{in}}).
\end{aligned}
$$

In addition, if $x(t=0) = y(t=0) = z_P(t=0) > 0$ and $\dot{x}(t=0) = \dot{y}(t=0) = \dot{z}_P(t=0) = 0$, then $x(t = t_{\text{in}}) = y(t = t_{\text{in}}) = z_P(t = t_{\text{in}}) = 0$ and $\dot{x}(t = t_{\text{in}}) = \dot{y}(t = t_{\text{in}}) = \dot{z}_P(t = t_{\text{in}}) = -\sqrt{2 \cdot g \cdot z_P(t=0)}$. Similarly, if the robot is able to jump out of water, and if the exit time instant is referred as t_{out}, the energy of the robot at the moment of exit is (note that the robot's foot at the moment of exit is out of water):

$$
\begin{aligned}
&E_{\text{out}} = E\left(t = t_{\text{out}}\right) = K_1\left(t_{\text{out}}\right) + K_2\left(t_{\text{out}}\right) + K_3\left(t_{\text{out}}\right) + U_{g,1}\left(t_{\text{out}}\right)\\
&\quad + U_{g,2}\left(t_{\text{out}}\right) + U_{g,3}\left(t_{\text{out}}\right) + U_k(t_{\text{out}}),\\
&K_1 = \frac{m_1 \cdot \dot{x}_{\text{out}}^2}{2}; \quad U_{g,\,1} = m_1 \cdot g \cdot x_{\text{out}}; \quad K_2 = \frac{m_1 \cdot \dot{y}_{\text{out}}^2}{2}; \quad U_{g,\,2} = m_2 \cdot g \cdot y_{\text{out}};\\
&K_2 = \frac{m_1 \cdot \dot{z}_{P,\text{out}}^2}{2}; \quad U_{g,\,3} = m_2 \cdot g \cdot z_{P,\,\text{out}} \overbrace{=}^{z_P(t_{\text{out}})=0} 0;\\
&\quad U_k = \frac{1}{2} \cdot k \cdot \left(x_{\text{out}} - z_{P,\,\text{out}}\right)^2 \overbrace{=}^{z_P(t_{\text{out}})=0} \frac{1}{2} \cdot k \cdot x_{\text{out}}^2
\end{aligned}
\tag{16}
$$

https://doi.org/10.1017/S0263574714002495 Published online by Cambridge University Press

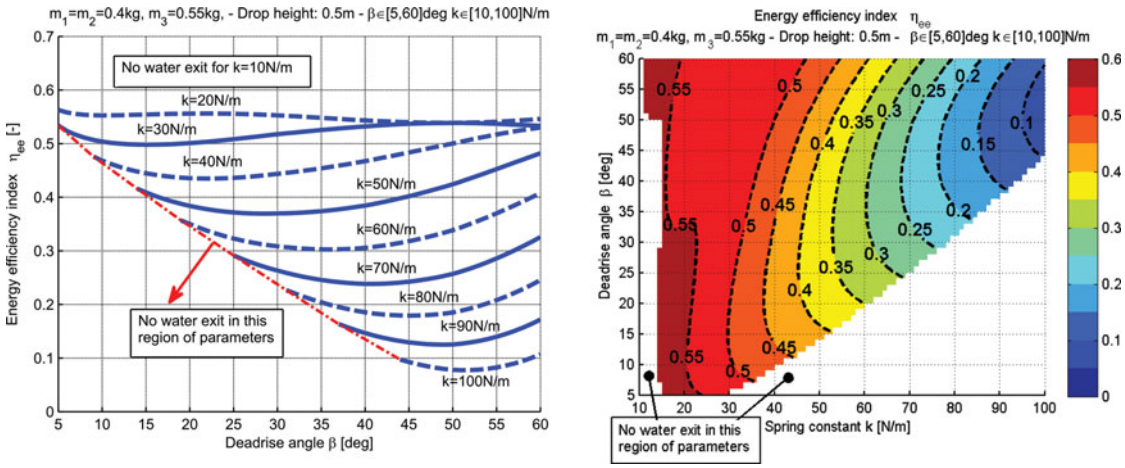


Fig. 8. Simulation of a passive free fall, single jump test. Left: Energy efficiency index η_{ee} versus deadrise angle β for different values of spring constant k. Right: Contour plot of energy efficiency index η_{ee} as a function of deadrise angle β and spring constant k.

with

$$x_{out} = x\,(t_{out})\,; \quad \dot{x}_{out} = \dot{x}\,(t_{out})\,;$$
$$y_{out} = y\,(t_{out})\,; \quad \dot{y}_{out} = \dot{y}\,(t_{out})\,;$$
$$z_{P,\,out} = z_P\,(t_{out})\,; \quad \dot{z}_{P,\,out} = \dot{z}_P(t_{out}).$$

In case the robot is able to passively jump out of water, an energy efficiency index η_{ee} can therefore be defined as follows:

$$\eta_{ee} = \frac{E_{out}}{E_{in}}. \tag{17}$$

On the other hand, if the robot is not able to passively jump out of water, the energy efficiency index η_{ee} is undefined.

The energy efficiency index η_{ee} has been determined numerically for different values of deadrise angle β and spring coefficient k, keeping the mass parameters fixed to $m_1 = m_2 = 0.4$ kg and $m_3 = 0.55$ kg. Results of calculation are shown in Fig. 8, which reports, on the left, a plot of η_{ee} as a function of β for different values of k, and on the right, the contour plot of η_{ee} in the plane (k, β). It can be seen that for a fixed deadrise angle β, there is a tendency for η_{ee} to increase as the spring become softer, i.e. as k decreases. However, when k decreases too much, there is no longer a water exit (see the case with $k = 10$ N/m). Moreover, for a fixed value of the spring constant k, there is a limiting deadrise angle β below which there is no longer a water exit. The combinations of spring constant and deadrise angle, which actually lead to a possible passive jump, i.e. passive water exit after impact, can be clearly identified from the contour plot reported in the figure.

Results in Fig. 8 indicate that a soft, although not extremely soft, spring could be the optimum choice to achieve a high energy efficiency index. However, other parameters influence the practicability of the concept. Indeed, in order to keep the jumping robot as small as possible, it is necessary to limit the extreme sinkage z_P (which influences the overall required minimum height of the cone H_{cone} to avoid full submergence or water overtopping) and it is also necessary to limit the extreme elongation $x - z_P$ (which influences the overall size of the robot). In addition, the deadrise angle should be controlled, and it should be kept sufficiently large because small values of the deadrise angle tend to increase the overall size of robot since small deadrise angles are associated with large cone radii.

Figure 9 (left) shows the extreme sinkage z_P within a jump, i.e. in the period $t \in [t_{in}, t_{out}]$ for those conditions where the robot is able to jump out of water in a free fall passive drop test, while Fig. 9 (right) shows the contour plot of the extreme sinkage z_P in the plane (k, β). This analysis is associated with the concept that a robot which has a high *energy efficient index* is useless if its foot (cone's tip) sinks deeply into the water. Large scale water running robots should have the capacity to move on the water, exploiting just the surface layer (from 10 to 30 cm) of water. As a reference,

https://doi.org/10.1017/S0263574714002495 Published online by Cambridge University Press

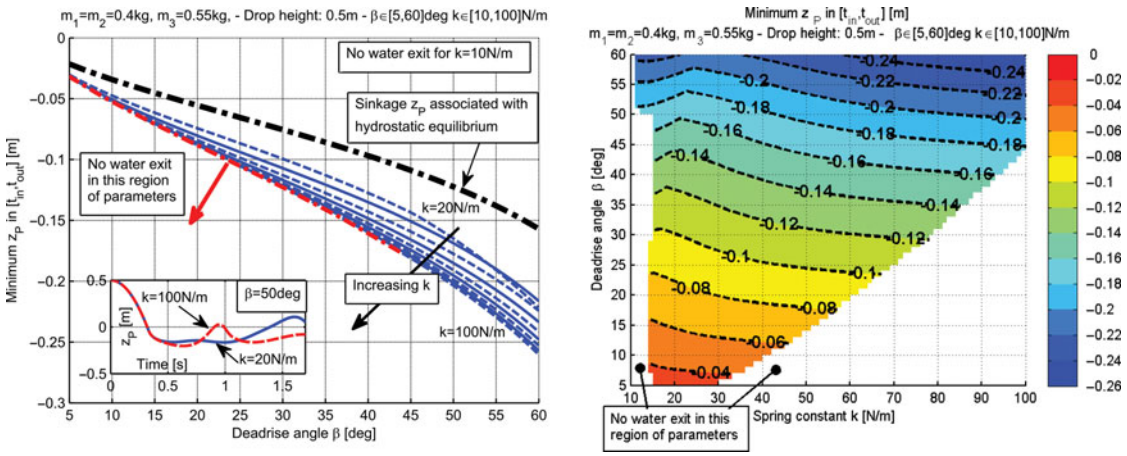


Fig. 9. Simulation of a passive free fall, single jump test. Left: Extreme sinkage versus deadrise angle β for different values of spring constant k. Right: Contour plot of extreme sinkage as a function of deadrise angle β and spring constant k.

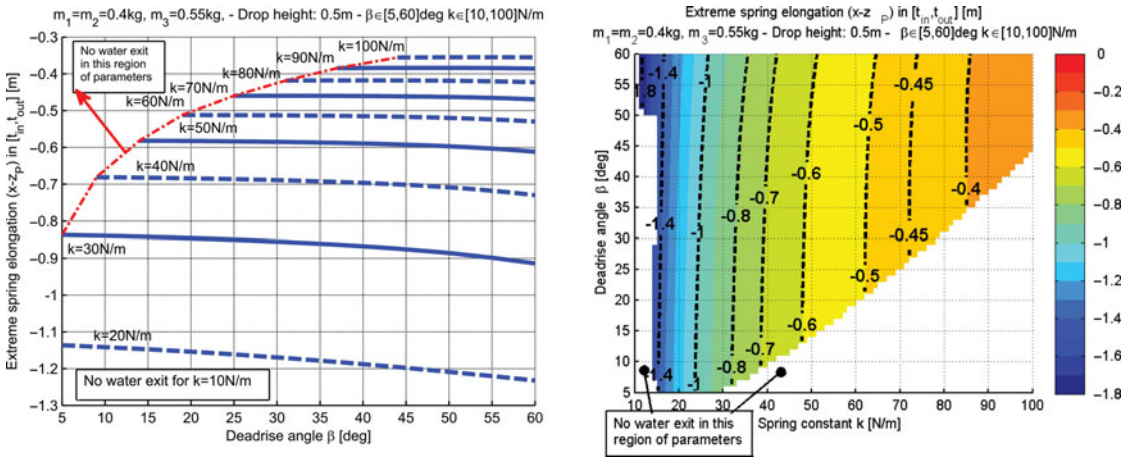


Fig. 10. Simulation of a passive free fall, single jump test. Left: Extreme spring elongation $(x - z_P)$ versus deadrise angle β for different values of spring constant k. Right: Contour plot of extreme spring elongation $(x - z_P)$ as a function of deadrise angle β and spring constant k.

in the same graph, the sinkage associated with the hydrostatic equilibrium is also reported. Looking at Fig. 9, for the considered configuration of masses, it can be noted that, as usual, the maximum dynamic sinkage exceeds the hydrostatic equilibrium sinkage due to dynamic effects that lead to the transformation of part of the original robot's energy into energy associated with the buoyancy force. Also, it can be seen that larger spring constants lead to larger extreme sinkage. Although this, at a first glance, could seem to be counterintuitive, the reason for this result is to be sought in the details of the oscillatory behavior of the system during the jump, i.e. in the period $t \in [t_{\text{in}}, t_{\text{out}}]$. A clarifying example comparison is shown in the sub-plot in Fig. 9 (left), where time histories $z_P(t)$ are compared when $k = 20$ and 100 N/m for the same deadrise angle $\beta = 50^\circ$.

As mentioned, another important aspect of the jumping action is the extreme spring elongation $x - z_P$, since such elongation influences the overall size of the robot. Large values of spring elongation are reflected in very bulk and, ultimately, mechanically inefficient robots. This quantity has therefore been analyzed in Fig. 10 by reporting the extreme spring elongation within a jump, i.e. for $t \in [t_{\text{in}}, t_{\text{out}}]$ for those conditions when the robot is able to passively jump out of water. In case the cone does not exit water, the extreme spring elongation is conventionally assumed as undefined. From the results reported in Fig. 10, it can be noted that, as expectable, softer springs are associated with large extreme spring elongations during the jump while being also associated with higher energy efficiency indices (see Fig. 8).

https://doi.org/10.1017/S0263574714002495 Published online by Cambridge University Press

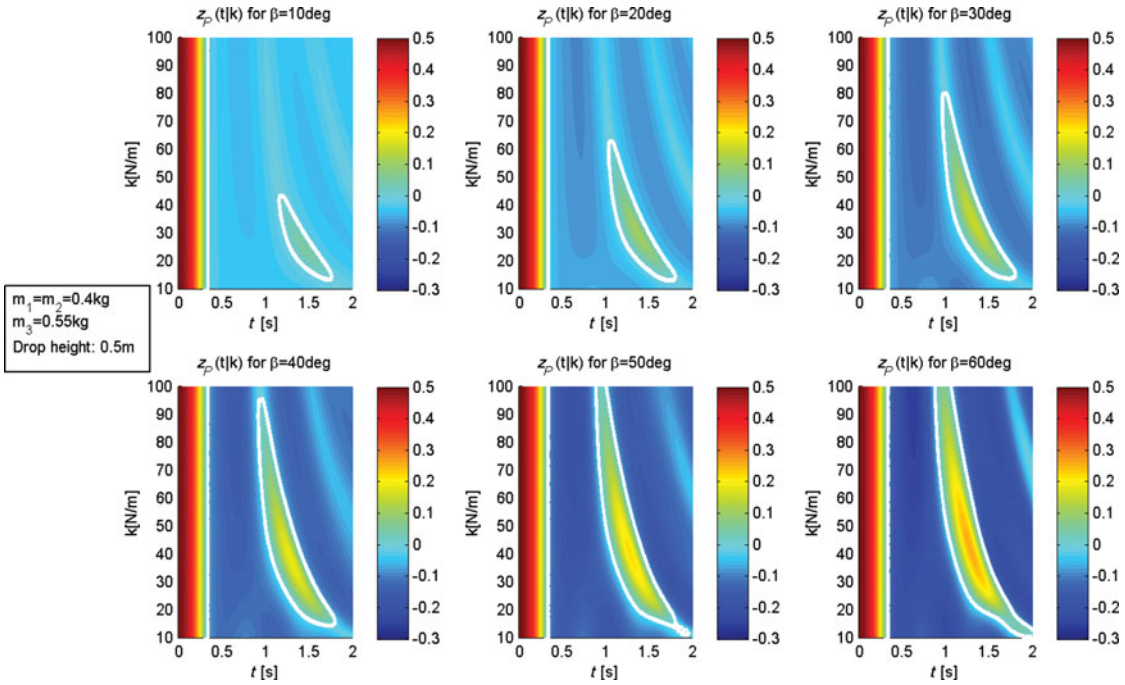


Fig. 11. Simulation of a passive free fall, single jump test. Surfaces of time history of $z_P(t|k)$ for different values of deadrise angle β and spring constant k.

Summarizing results in Figs. 8–10, the first general qualitative guideline regarding the effect of β and k can be inferred. In fact, the higher the β and $1/k$ (sharp cone coupled with a very soft spring), the higher the energy efficiency index η_{ee} (Fig. 8). On the other hand, if β is too large, the maximum cone's tip sinkage becomes significant (up to 25 cm for large β values as shown in Fig. 9). Moreover, if k is too small, the maximum spring elongation reaches unacceptable values (above 1.2 m for $k = 20$ N/m as shown in Fig. 10). Furthermore, if the spring constant is further reduced, the robot is no longer able to jump out of water. These plots suggest that β and k should be chosen to pursue a trade-off between jumping efficiency, low sinkage values, and overall size of the robot.

In addition to the above, it is worth to further analyze in more detail the behavior of $z_P(t)$ when the deadrise angle β and the spring constant k are varied. To do so, surfaces of the time history of $z_P(t|k)$ are shown in Fig. 11 for a series of values of β, from 10° to 60°. In Fig. 11, each surface section at a specific value of the spring constant k represents the time history $z_P(t|k)$ obtained for that value of the spring constant. In such a way, Fig. 11 provides a full overview of the behavior of the motion $z_P(t|k)$ when the spring constant k is changed. In all the cases the robot is initially released from a height of 0.5 m. In the figure, regions where the base of the robot is out of water are bound by white thick lines, corresponding to contours at $z_P(t|k) = 0$. By looking at the results in Fig. 11, it can be seen that when the deadrise angle is small, the region of the plane (t, k) where the robot can jump out of water is limited (compare, for instance., the top left plot for $\beta = 10°$ and the lower bottom plot for $\beta = 60°$). In addition, the height of the jump, i.e. the maximum value of z_P is also small. On the other hand, when the deadrise angle is increased, the region of the plane (t, k) where the robot is able to jump out of water increases. In particular, the region tends to extend toward the higher values of the spring constant k. In addition, the maximum jumping height above water also increases as the deadrise angle increases. It can also be noted that for sufficiently high values of deadrise angle, for the considered configuration of masses and dropping height, the maximum jumping height is obtained for spring constants around 40 N/m.

6.2. Forced motion, multiple jumps case

In order to gain an insight into the phenomenon of water bouncing of 2-DoF mechanism, a multiple jumps simulation has been carried out. In the simulation, a dynamic forcing is introduced through

https://doi.org/10.1017/S0263574714002495 Published online by Cambridge University Press

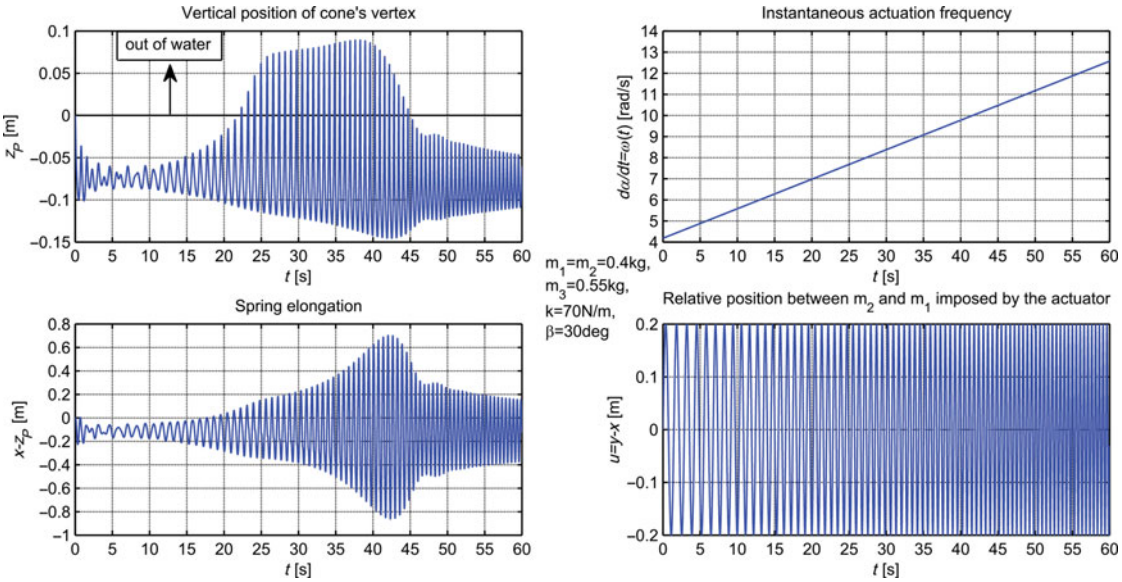


Fig. 12. Time history of example-forced motion with sweep frequency actuation.

the action of an actuator, which imposes the relative motion u between mass m_2 and m_1 (see Eq. (1)). Actuator action is responsible for the robot bouncing off water, which occurs only under certain conditions.

In the simulation, the actuator imposes the motion u having the following form:

$$u = A \cdot \sin(\alpha(t)), \tag{18}$$

where the forcing amplitude A is assumed to be constant. During the simulation, the driving phase $\alpha(t)$ is slowly increased to obtain a linear chirp input signal. This occurs when

$$\alpha(t) = \omega_0 \cdot t + \frac{1}{2} k_\omega \cdot t^2 \Rightarrow \omega(t) = \frac{d}{dt}\alpha(t) = \omega_0 + k_\omega \cdot t, \tag{19}$$

where $\omega(t)$ (rad/s) is the instantaneous forcing frequency, ω_0 (rad/s) is the initial driving frequency, and k_ω (rad/s^2) is a constant, which represents the rate of increase of frequency or chirp rate. The relationship between k_ω, initial driving frequency ω_0, final driving frequency ω_f, and total time of simulation T is

$$k_\omega = \frac{\omega_f - \omega_0}{T}. \tag{20}$$

In the performed simulation example, robot's mass has been chosen as $m_1 = m_2 = 0.4$ kg and $m_3 = 0.55$ kg, with a spring constant, $k = 70$ N/m and a deadrise angle $\beta = 30^\circ$. The actuation frequency varies linearly from $\omega_0 = 4.18$ to 12.57 rad/s in a total time $T = 60$ s, with a forcing amplitude $A = 0.20$ m. The robot is initially released from the water surface. Results from the simulation are shown in Fig. 12.

Since the water level is assumed to be nominal at $z = 0$, the cone's tip jumps off the water when $z_P > 0$. Looking at the results in Fig. 12, it can be noted that the cone jumps off the water after 22 s and keeps jumping off until about 45 s. These two time points correspond to two limit driving frequencies, namely 7.3 and 10.5 rad/s. Outside these frequencies, the mechanical system is not able to jump off the water. Also note that the optimum result in terms of jumping effect is not obtained when the mass/spring system achieves maximum elongation (around 42 s).

https://doi.org/10.1017/S0263574714002495 Published online by Cambridge University Press

This example result immediately reaches the conclusion that particular care is required in the choice of dynamic parameters such as mechanism's mass, stiffness, and, in particular, driving frequency.

7. Conclusions

The paper presented the modeling and simulation of a 2-DoF water bouncing robot. The simulation is based on the dynamical model of the masses and spring involved in the mechanism. A simplified analytical model of fluid-structure interaction force has been proposed as well for both water-entry and water-exit phases. The model has been validated through experimental results.

Eventually, a simulation of the whole system (2-DoF mechanism integrated with the fluid-structure interaction force model) has been carried out.

The simulation showed that to make the robot jump off the water, particular care is required in the choice of dynamic parameters such as masses of mechanism, stiffness, and, in particular, driving frequency. In particular, notwithstanding the limitations coming from the applied simplified modeling, some observed features of the problem are worth being highlighted to provide some possible indications for a "good design."

First of all, it shall be reported that not all the combinations of deadrise angle β and spring constant k allow passive jumping (single jump case) out of water for the tested case. Given the deadrise angle, the passive jumping out of water has been observed by simulations in a range of spring constants. Such range of spring constants depends on the deadrise angle itself.

From the point of view of practical design, the most likely interesting limitation for the occurrence of passive jumping out of water for a given deadrise angle is the observed maximum allowable spring constant. Higher spring constants can be desirable to limit the overall size of the system because higher spring constants reduce extreme spring elongation after the impact, and thus the overall size of the system. However, given the deadrise angle, an upper limit has been observed for the spring constant, above which passive jumping out of water no longer occurs. Such upper limitation of the spring constant increases as the deadrise angle increases. On the other hand, although increase in spring constant is able to limit the maximum elongation of spring after the impact, the maximum sinkage of robot's foot is not very much affected by the spring constant. Instead, the maximum sinkage of robot's foot is mostly influenced by the deadrise angle. This is explained by the fact that the maximum sinkage of robot's foot is significantly governed by buoyancy effects. In general, increase in spring constant, while having positive effect of limiting the overall size of the mechanism, has the side effect of reducing the energy efficiency of the system.

When considering the simulations carried out in forced conditions (case of multiple jumps), the possibility of obtaining a jumping is the result of delicate tuning between system's and forcing characteristics. Such tuning is complicated by the fact that the system acts as a linear system when it is completely out of water, while it behaves as a nonlinear system when robot's foot is in water. In the considered example, given the forcing amplitude, jumping out of water has been obtained by simulations only in a limited range of forcing frequencies.

We hope that our results can offer the first useful contribution to the research field of large scale water running robots.

Acknowledgements

We would like to thank Lorenzo Scalera for his help at several stages of the current work.

References

1. J. W. M. Bush and D. L. Hu, "Walking on water: Bio-locomotion at the interface," *Annu. Rev. Fluid Mech.* **38**, 339–369 (2006).
2. G. De Backer, M. Vantorre, C. Beels, J. De Pré, S. Victor, J. De Rouck, C. Blommaert and W. Van Paepegem, "Experimental investigation of water impact on axisymmetric bodies," *Appl. Ocean Res.* **31**, 143–156 (2009).
3. O. M. Faltinsen, *Hydrodynamics of High Speed Marine Vehicles* (Cambridge University Press, Cambridge, UK, 2005).
4. O. Faltinsen and R. Zhao, "Water Entry of Ship Sections and Axisymmetric Bodies," *Proceedings of the AGARD FDP Workshop on High Speed Body Motion in Water*, Kiev, Ukraine (Sep. 1–3, 1997) pp. 24-1–24-11.

https://doi.org/10.1017/S0263574714002495 Published online by Cambridge University Press

5. S. Floyd and M. Sitti, "Design and development of the lifting and propulsion mechanism for a biologically inspired water runner robot," *IEEE Trans. Robot.* **24**(3), 698–709 (2008).
6. S. Floyd, S. Adilak, S. Ramirez, R. Rogman and M. Sitti, "Performance of Different Foot Designs for a Water Running Robot," *Proceedings – IEEE International Conference on Robotics and Automation*, 4543216 (2008) pp. 244–250.
7. J. W. Glasheen and T. A. McMahon, "Size-dependence of water-running ability in basilisk lizards (Basiliscus basiliscus)," *J. Exp. Biol.* **199**, 2611–2618 (1996a).
8. J. Glasheen and T. McMahon, "A hydrodynamic model of locomotion in the basilisk lizard," *Nature* **380**, 340–342 (1996b).
9. J. Glasheen and T. McMahon, "Vertical water entry of disks at low Froude numbers," *Phys. Fluids* **8**, 2078–2083 (1996c).
10. S. P. Hyun, S. Floyd and M. Sitti, "Dynamic Modelling of a Basilisk Lizard-Inspired Quadruped Robot Running on Water," *Proceedings of the IEEE/RSJ International Conference on Intelligent Robots and Systems (IROS)*, 4651084 (2008) pp. 3101–3107.
11. H. Lamb, *Hydrodynamics*, 6th ed. (Cambridge University Press, Cambridge, UK, 1932).
12. P. A. Martin, "On the added mass of rippled discs," *J. Eng. Math.* **33**, 421–435 (1998).
13. J. Pandey, N. S. Reddy, R. Ray and S. N. Shome, "Biological Swimming Mechanism Analysis and Design of Robotic Frog," *IEEE International Conference on Mechatronics and Automation (IEEE ICMA 2013)*, 6618176 (2013) pp. 1726–1731.
14. D. Piro and K. J. Maki, "Hydroelastic Wedge Entry and Exit," *Proceedings of the 11th International Conference on Fast Sea Transportation (FAST 2011)*, Honolulu, Hawaii (Sep. 2011).
15. Y. M. Scolan and A. A. Korobkin, "Three-dimensional theory of water impact, part 1 inverse wagner problem," *J. Fluid Mech.* **440**, 293–326 (2001).
16. B. Shin, H.-Y. Kim and K.-J. Cho, "Towards a Biologically Inspired Small-Scale Water Jumping Robot," *2nd Biennial IEEE/RAS-EMBS International Conference on Biomedical Robotics and Biomechatronics (BioRob 2008)*, 4762896 (2008) pp. 127–131.
17. T. Von Karman, "The Impact on Seaplane Floats during Landing," *Tech. Note No. 321* (NACA, Washington, 1929).
18. L. Wang, T. Gao, F. Gao, L. Dong and J. Wu, "Dynamic Research on a Water Walking Robot Inspired by Water Striders," *Proceedings of the Second International Symposium on Computer Science and Computational Technology*, Huangshan, P.R. China (Dec. 26–28, 2009) pp. 439–442.
19. H. Wagner, "Über stoss und gleitvorgänge an der oberfläche von Flüssigkeiten," *Z. Angew. Math. Mech.* **12**(4), 193–235 (1932).
20. X. Zhang, J. Zhao, Q. Zhu, N. Chen, M. Zhang and Q. Pan, "Bioinspired aquatic microrobot capable of walking on water surface like a water strider," *ACS Appl. Mater. Interfaces* **3**(7), 2630–2636 (2011).
21. J. Zhao, X. Zhang, N. Chen and G. Pan, "Why superhydrophobicity is crucial for a water-jumping microrobot? Experimental and theoretical investigations," *ACS Appl. Mater. Interfaces* **4**(7), 3706–3711 (2012).

https://doi.org/10.1017/S0263574714002495 Published online by Cambridge University Press